Probing CP Structure of ALPs at Future Lepton Colliders

Jian-Nan Ding,Yan-Dong Liu, Mu-Yuan Song

Muyuan Song

State Key Laboratory of Nuclear Physics and Technology,
Institute of Quantum Matter,
South China Normal University

July 28th, 2025

The Fourth International Conference on Axion Physics and Experiment (Axion 2025)

Axion-like particles (ALPs)

- A pseudo-Nambu-Goldstone boson arose from broken global PQ symmetry (QCD-axion).
- More broader parameter space than QCD axion (free mass-coupling relation, f_a, m_a).

$\rightarrow$ String theory [P. Svrcek, E. Witten, 2006], collider/beamdump exploration [M. Bauer, M.Neubert,2017;J. D. Bjorken, et. al., 1988].

- CP violation is essential for baryon asymmetry (matter-antimatter asymmetry).
- ALP-photon interactions probe CP violation at high-energy colliders (comparison with eEDMs)

Effective Lagrangian

$$\mathcal{L} \supset \frac{1}{2}(\partial_\mu a)^2 - \frac{1}{2}m_a^2 a^2 + \frac{\tilde{C}_\gamma}{\Lambda} a F_{\mu\nu}\tilde{F}^{\mu\nu} + \frac{C_\gamma}{\Lambda} a F_{\mu\nu}F^{\mu\nu}$$

CP nature of ALPs at low energy exp constraints

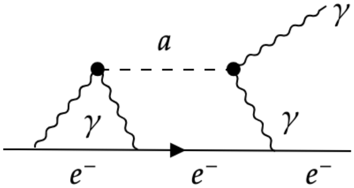

- The product $C_\gamma \tilde{C}_\gamma$ is constrained, $d_e/e \simeq -\frac{3\,\alpha\, Q_e^3}{\pi^3} \frac{m_e}{\Lambda^2} C_\gamma \tilde{C}_\gamma \log^2 \frac{\Lambda}{m_a}$ [L. Di Luzio, et al. PRD. 104 (2021) 095027].
- $|d_e| < 1.1 \times 10^{-29}$ e cm (ACME) [Nature 562 (2018) 355]
- $|d_e| < 4.1 \times 10^{-30}$ e cm (JILA) [Science 381 (2023) 6653]
- Collider experiments would also probe the CP-violating phenomena by using kinematic observables.

Target Process at Lepton Colliders

Effective Lagrangian

$$\mathcal{L} \supset \frac{1}{2}(\partial_\mu a)^2 - \frac{1}{2}m_a^2 a^2 + \frac{\tilde{C}_\gamma}{\Lambda} a F_{\mu\nu}\tilde{F}^{\mu\nu} + \frac{C_\gamma}{\Lambda} a F_{\mu\nu}F^{\mu\nu}$$

- $\frac{C_\gamma}{\Lambda}$: CP-odd; $\frac{\tilde{C}_\gamma}{\Lambda}$: CP-even

Signal Process

$$e^+e^- \to e^+e^-a \to e^+e^-\gamma\gamma$$

- $\sqrt{s} = 240$ GeV lepton collider (CEPC/ILC/FCC-ee), $\mathcal{L}_{\text{int}} = 5$ ab^{-1}.
- ALP production via VBF and s-channel
- VBF dominance: s-channel contribution suppressed by large $\sqrt{s}$.

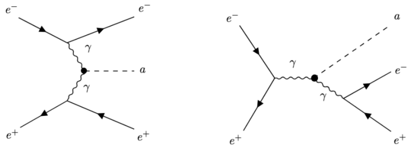

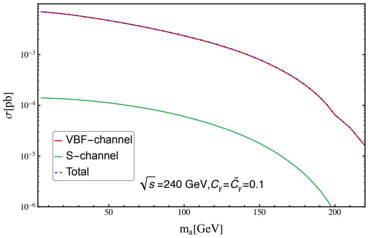

Figure: Comparison of VBF(red) and s-channel(green) contributions, $\Lambda = 1$ TeV

Target Process at Lepton Colliders

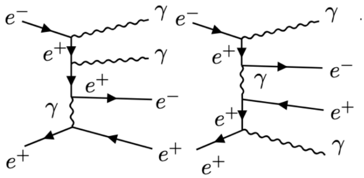

Background Process

Dominant QED $e^+e^- \to e^+e^-\gamma\gamma$

- h, Z contributions are suppressed by the masses and LBL is effectively dominant for small ALPs $(m_a < 5$ GeV$)$[Patricia R. Teles, et.al, Phys.Rev.D 109 (2024) 5, 5].
- Rare heavy hadron decays enhance production rates of small ALPs. (we only focus on diphoton events $\to 5 \sim 220$ GeV)
- Detector simulation: FeynRules + MadGraph + Delphes

CP-sensitive Observable: $\Delta\phi_{ee}$

$$\Delta\phi_{ee} = \phi_{e^+} - \phi_{e^-}$$

- ϕ_i is the azimuthal angle of the particle momentum (relative to the beam axis).
- The asymmetric feature offers the sensitivity to coexistence of CP-even and CP-odd couplings (see orange).

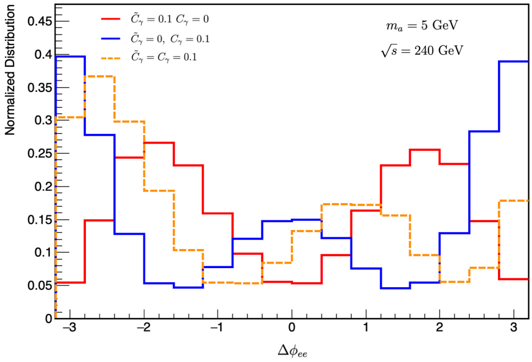

Figure: Azimuthal angular distribution $\Delta\phi_{ee}$ for e^+e^- pairs (parton level).

Cut-based Strategy: Low and High mass region

Low Mass Region ($5 \leq m_a \leq 120$ GeV)

- $N_e = 2, N_\gamma = 2$
- $p_T^{\gamma_1} > 20$ GeV, $p_T^{\gamma_2} > 15$ GeV, $|\eta_\gamma| < 1.0$, $\Delta R_{e\gamma} > 1.5$
- $\Delta\eta_{ee} > 2.0$, $m_{ee} > 100$ GeV
- $|m_{\gamma\gamma} - m_a| < 1$ GeV

High Mass Region ($120 < m_a \leq 220$ GeV)

- $N_e = 2, N_\gamma = 2$
- $p_T^{\gamma_1} > 40$ GeV, $p_T^{\gamma_2} > 25$ GeV, $|\eta_\gamma| < 1.0$, $\Delta R_{e\gamma} > 1.0$
- $\Delta\eta_{ee} > 1.0$
- $|m_{\gamma\gamma} - m_a| < 2$ GeV

$$\Delta R_{ij} = \sqrt{(\phi_i - \phi_j)^2 + (\eta_i - \eta_j)^2}$$

- Final-state selection; Photon kinematics; VBF-dominant selection; and the ALP-mass window (narrow diphoton mass reconstruction).
- Last two are the strong cuts.

Table: Cutflow for low-mass ALP signals (assuming $\tilde{C}_\gamma = C_\gamma = 0.1$) and SM backgrounds.

Cuts	Cross section for signal (background) [pb]		
	$m_a = 5$ GeV	$m_a = 50$ GeV	$m_a = 90$ GeV
Pre-selection	3.09×10^{-3} (0.082)	3.77×10^{-3} (0.082)	2.54×10^{-3} (0.082)
Cut 1	2.73×10^{-3} (0.058)	3.31×10^{-3} (0.058)	2.20×10^{-3} (0.058)
Cut 2	1.25×10^{-3} (1.67×10^{-3})	1.14×10^{-3} (1.67×10^{-3})	7.42×10^{-4} (1.67×10^{-3})
Cut 3	8.76×10^{-4} (2.61×10^{-4})	8.43×10^{-4} (2.61×10^{-4})	5.05×10^{-4} (2.61×10^{-4})
Cut 4	8.73×10^{-4} (2.10×10^{-6})	7.20×10^{-4} (8.31×10^{-6})	3.47×10^{-4} (2.41×10^{-6})

Cut table (2)

Table: Cutflow for high-mass ALP signals (assuming $\tilde{C}_\gamma = C_\gamma = 0.1$) and SM backgrounds.

Cuts	Cross section for signal (background) [pb]		
	$m_a = 125$ GeV	$m_a = 170$ GeV	$m_a = 200$ GeV
Pre-selection	1.42×10^{-3} (0.081)	3.85×10^{-4} (0.081)	6.19×10^{-5} (0.081)
Cut 1	1.16×10^{-3} (0.057)	3.06×10^{-4} (0.057)	4.60×10^{-5} (0.057)
Cut 2	5.81×10^{-4} (1.41×10^{-3})	1.46×10^{-4} (1.41×10^{-3})	1.88×10^{-5} (1.41×10^{-3})
Cut 3	4.96×10^{-4} (4.51×10^{-4})	1.10×10^{-4} (4.51×10^{-4})	9.91×10^{-6} (4.51×10^{-4})
Cut 4	4.76×10^{-4} (1.1×10^{-5})	9.61×10^{-5} (1.71×10^{-6})	7.97×10^{-6} (3.24×10^{-7})

Likelihood Analysis

- Binned likelihood analysis for normalized differential $\Delta\phi_{ee}$.
- Comparison with existing eEDM constraints (90% C.L. exclusion significance), σ_{exc}:

$$\sigma_{\text{exc}} = \sqrt{-2\ \ln\left(\frac{L(S+B|B)}{L(B|B)}\right)} \geq 1.65,$$

$$L(x|y) = \prod_i^N \frac{x_i^{y_i}}{y_i!} e^{-x_i},$$

$$S = S_\gamma + \tilde{S}_\gamma + S_{\tilde{\gamma}\gamma} \propto \frac{|C_\gamma|^2}{\Lambda^2}|\mathcal{M}_{aFF}|^2 + \frac{|\tilde{C}_\gamma|^2}{\Lambda^2}|\mathcal{M}_{a\tilde{F}F}|^2 + 2\frac{C_\gamma\tilde{C}_\gamma}{\Lambda^2}\text{Re}[\mathcal{M}^*_{a\tilde{F}F}\mathcal{M}_{aFF}]$$

CP-even, affecting production cross-section of ALPs

CP-odd, induce an asymmetric distribution in $\Delta\phi_{ee}$

Normalized differential $\Delta\phi_{ee}$ and 2D plane vs. eEDM

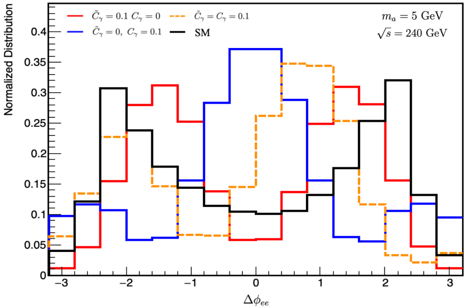

Figure: Normalized differential dis. $\Delta\phi_{ee}$ after selection cut for $m_a = 5$ GeV (reconstruction level). C_γ(blue),$\tilde{C}_\gamma$(red),$C_\gamma = \tilde{C}_\gamma$ (orange).

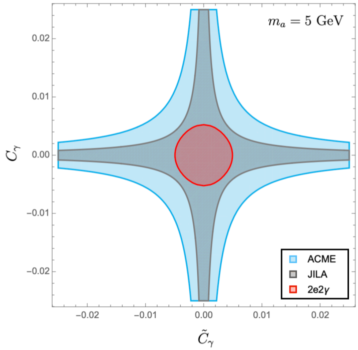

Figure: 2D constraints for the ALP-diphoton against eEDM constraints(ACME,JILA)

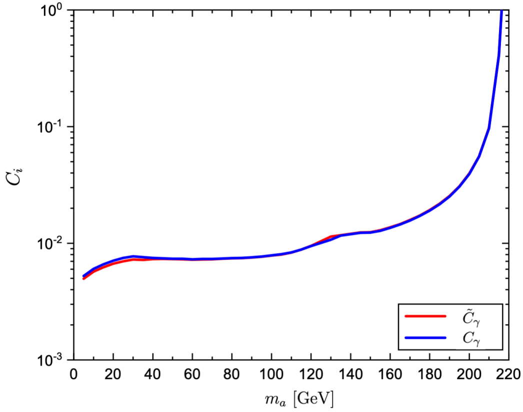

Figure: Single coupling $C_\gamma/\tilde{C}_\gamma$.

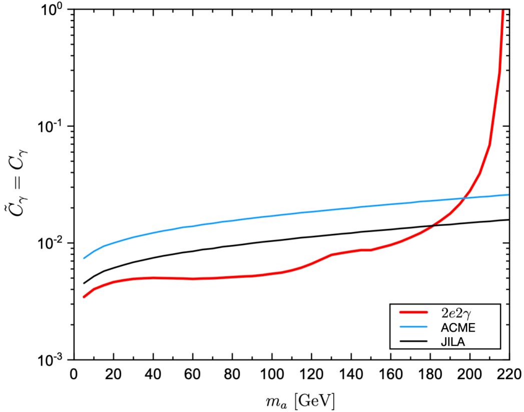

Figure: Equal couplings $C_\gamma = \tilde{C}_\gamma$ against eEDM constraints

- Test the dominant CP component of the signal against the discovery signal. Determine the region which operator $(C_\gamma/\tilde{C}_\gamma)$ dominates the $\Delta\phi_{ee}$ shape.

$$\sigma_{\text{dis}} = \sqrt{-2\ln\left(\frac{L(B|S+B)}{L(S+B|S+B)}\right)} \geq 5,$$

$$\sigma_{\tilde{C}_\gamma} = \sqrt{-2\ln\left(\frac{L(\tilde{S}_\gamma+B|S+B)}{L(S+B|S+B)}\right)} \leq 2, \text{ CP-even dominant}$$

$$\sigma_{C_\gamma} = \sqrt{-2\ln\left(\frac{L(S_\gamma+B|S+B)}{L(S+B|S+B)}\right)} \leq 2, \text{ CP-odd dominant}$$

- If the ALP is discovered, the discriminating power of differential $\Delta\phi_{ee}$ with and without CP-violating interaction can be tested.

CP structure sensitivity

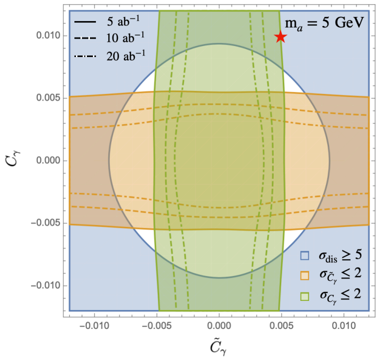

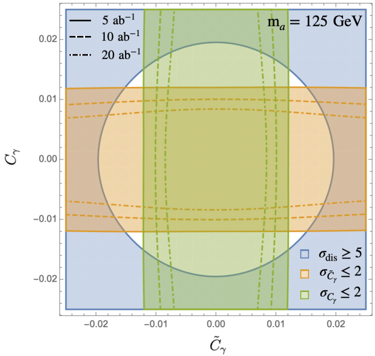

- Blue region (5 σ discovery), Orange and green represent the single operator dominance of $\Delta\phi_{ee}$.
- Diagonal direction ($C_\gamma \sim \tilde{C}_\gamma$), both contribute to the observed $\Delta\phi_{ee}$.
- Higher luminosity enhances CP violation detectability (see red star).

Summary

- Future lepton colliders offer opportunities to probe ALPs and sensitivity to test CP structure.
- The kinematic observable, $\Delta\phi_{ee}$, where the shape structure reveals CP nature and could surpass the recent eEDM bounds.
- Pure C_γ or $\tilde{C}_\gamma \neq 0$ CP-conserving scenarios reach $\mathcal{O}(10^{-2})$ TeV^{-1}, while CP-violating $C_\gamma = \tilde{C}_\gamma \neq 0$ reach $\mathcal{O}(10^{-3})$ TeV^{-1} couplings.
- $\Delta\phi_{ee}$ reveals the interference feature when both operators exist after the discovery of ALPs.
- Enhanced luminosity would improve the ability to probe CP-violation.

Thank you!

Main background

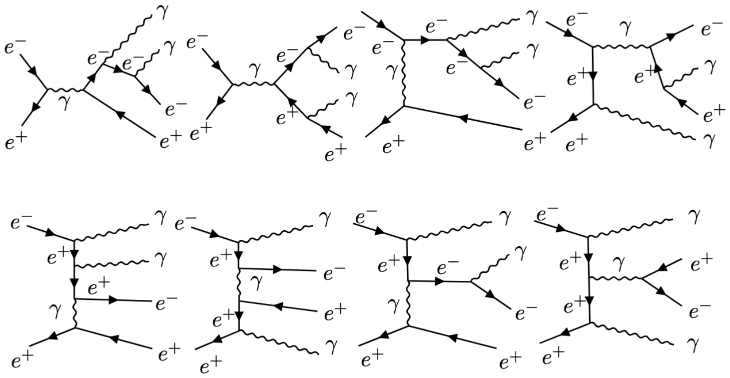

Figure: QED $e^+e^- \to e^+e^-\gamma\gamma$

ALP Decay Length(1)

$$\Gamma_a = \frac{\left(C_\gamma^2 + \tilde{C}_\gamma^2\right) m_a^3}{4\pi}$$

$$L_a = \frac{4\pi E_a}{(C_\gamma^2 + \tilde{C}_\gamma^2) m_a^4}$$

- Typically $\mathcal{O}(\mu m)$ for weak couplings.
- Decays promptly to $\gamma\gamma$.

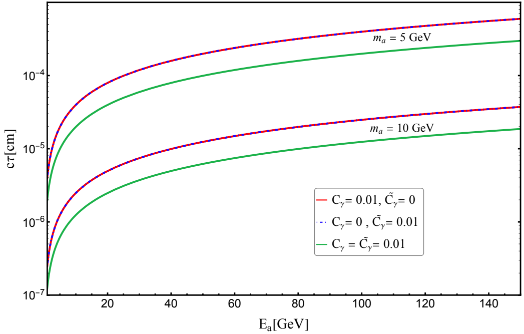

Figure: ALP decay length vs. mass

ALP Decay Length(2)

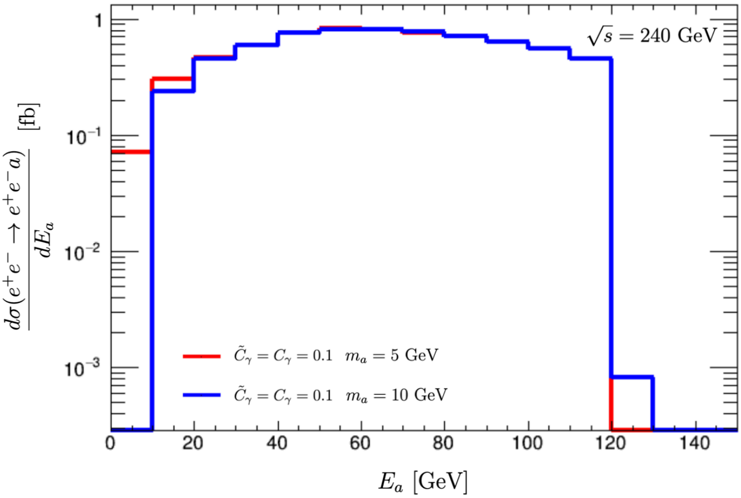

Figure: differential Xsection over energy of ALPs

Preselection of the signal and backgrounds

Low Mass Region ($5 \leq m_a \leq 120$ GeV)

- $p_T^\gamma > 10$ GeV, $p_T^\ell > 10$ GeV,
- $|\eta_\gamma| < 2.5$, $|\eta_\ell| < 2.5$,
- $\Delta R_{\gamma\gamma} > 0.1$, $\Delta R_{e\gamma} > 0.4$, $\Delta R_{\ell\ell} > 0.4$.

High Mass Region ($120 < m_a \leq 220$ GeV)

- $p_T^\gamma > 10$ GeV, $p_T^\ell > 10$ GeV,
- $|\eta_\gamma| < 2.5$, $|\eta_\ell| < 2.5$,
- $\Delta R_{\gamma\gamma} > 0.4$, $\Delta R_{e\gamma} > 0.4$, $\Delta R_{\ell\ell} > 0.4$.

Diphoton invariant mass cut

- photon energy resolution for future lepton colliders [*X. Ai et al, 2024; Y. Wang, 2022*],

$$\frac{\Delta E_\gamma}{E_\gamma} = \frac{3\%}{\sqrt{E_\gamma\,(\mathrm{GeV})}} \oplus 1\%.$$

- Good resolution benefits for the reconstruction of ALP diphoton mass.